







## Generalized relationship between effective forces and active particle microstructure

Xiaoting Yu,<sup>1</sup> Xue Zhang,<sup>1</sup> Yuxin Tian<sup>1</sup>,, Qun Zhang,<sup>1</sup> Peicheng Xu<sup>2</sup>,, Luhui Ning<sup>3,4,\*</sup>,, Ning Zheng<sup>1,†</sup>,  
Mingcheng Yang<sup>5,6,7,‡</sup>, and Peng Liu<sup>1,§</sup>,<sup>1</sup>*School of Physics, Beijing Institute of Technology, Beijing 100081, China*<sup>2</sup>*Wisdom Lake Academy of Pharmacy, Xi'an Jiaotong-Liverpool University, Suzhou 215123, China*<sup>3</sup>*Beijing Key Laboratory of Optical Detection Technology for Oil and Gas, China University of Petroleum-Beijing, Beijing 102249, China*<sup>4</sup>*Basic Research Center for Energy Interdisciplinary, College of Science, China University of Petroleum-Beijing, Beijing 102249, China*<sup>5</sup>*Beijing National Laboratory for Condensed Matter Physics and Laboratory of Soft Matter Physics, Institute of Physics, Chinese Academy of Sciences, Beijing 100190, China*<sup>6</sup>*School of Physical Sciences, University of Chinese Academy of Sciences, Beijing 100049, China*<sup>7</sup>*Songshan Lake Materials Laboratory, Dongguan, Guangdong 523808, China*

(Received 10 March 2025; accepted 1 July 2025; published 21 July 2025)

Establishing a robust link between microscopic structure and effective forces in active systems remains a fundamental challenge. Recently, Paul *et al.* [*Phys. Rev. Lett.* **129**, 058001 (2022)] achieved a significant theoretical breakthrough by developing a framework based on active stress. This framework enables the computation of forces exerted by active particles on a tightly constrained probe. Nevertheless, the pronounced sensitivity of depletionlike forces in active baths to external constraints offers an opportunity to extend this theoretical framework. Using simulations, we systematically investigate this constraint dependence and uncover key discrepancies between theory and numerical results. By incorporating a constraint-dependent correction factor into the existing theory, our results align remarkably well with simulations across extensive parameters. Our findings advance the theoretical understanding of depletionlike forces in active matter and offer direct implications for experimental validation.

DOI: [10.1103/rlp5-wxpf](https://doi.org/10.1103/rlp5-wxpf)

## I. INTRODUCTION

Active matter, observed in both natural systems, such as the cytoskeleton [1,2] and living organisms [3–14], and artificial systems, such as colloidal swimmers [15–20] and vibrating particles [21–24], breaks spatial and time-reversal symmetries, exhibiting a range of phenomena unattainable in thermal equilibrium [25–37]. To explore and understand the exceptional properties of active matter, fundamental physical concepts often need to be extended from thermal to active baths [38–46]. In equilibrium systems, effective depletion interactions between particles immersed in depletants or between large particles and system boundaries arise from entropy maximization [47,48]. Briefly, when larger objects approach each other, the entropy of an overwhelming number of depletants increases due to the expansion of accessible volume. However, in active baths, the interactions between passive particles are far more intricate. For instance, altering the density of active particles (APs) can cause the force exerted on two fixed objects by the APs to transition from long-range repulsion to long-range attraction, accompanied by nonmonotonic oscillatory behavior [37,49–57]. This oscillatory effective force as a function of interobject separation

originates from the dynamic layering of APs and the formation of dense microstructures between the objects [51,57]. Recent studies have shown that the effective interactions between two passive particles in an active bath are highly sensitive to the elastic or dynamic constraints imposed on them [58]. This is because the constraints influence the particle motion under collisions with APs, thereby changing the AP distribution around the passive particle. This constraint dependence is not limited to interparticle forces; it also governs other physical observables, including average potential energy, active noise, active depletion torque, and active pressure experienced by passive objects [59–62]. These findings underscore the distinct nature of physical concepts in active baths compared to equilibrium systems, providing new perspectives on the complex interactions within active systems.

A fundamental challenge in active systems is to theoretically establish a direct relationship between the microscopic structure of APs and the resulting depletionlike forces on immersed objects—analogue to equilibrium cases [63–67]. Recently, Paul *et al.* made remarkable progress by developing a theoretical framework based on active stress [68–71], enabling the computation of forces exerted by APs on a constrained probe within a circular cavity [72]. This force is governed by an effective temperature, which accounts for density fluctuations from particle activity, and by the integral of the nonequilibrium AP distribution, as confirmed by optical tweezer experiments. However, since optical tweezers impose constraints through harmonic potential wells [72], these constraints may fundamentally influence the measured

\*Contact author: [lhningphy@cup.edu.cn](mailto:lhningphy@cup.edu.cn)†Contact author: [ningzheng@bit.edu.cn](mailto:ningzheng@bit.edu.cn)‡Contact author: [mcyang@iphy.ac.cn](mailto:mcyang@iphy.ac.cn)§Contact author: [liupeng@bit.edu.cn](mailto:liupeng@bit.edu.cn)

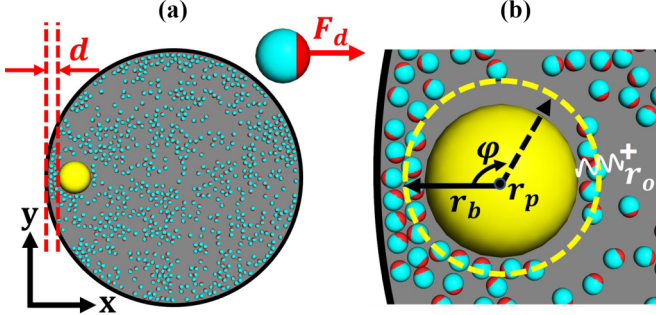


FIG. 1. (a) Schematic of the simulation system, consisting of small APs with a packing fraction  $\rho = 0.3$  and a passive spherical probe (yellow) placed at a surface-to-surface distance  $d$  from the circular confinement. Inset: The self-propelling motion of the APs toward the red region. (b) The passive probe is constrained by an external harmonic potential,  $U(\mathbf{r}_p) = \frac{1}{2}k(\mathbf{r}_p - \mathbf{r}_0)^2$ , where  $k$  is the trap stiffness and  $\mathbf{r}_0$  is the trap center. Additionally, the circular radius  $r_b$  and angle  $\varphi$ , which define the integration contour of the APs' density distribution, are illustrated for clarity.

forces, necessitating careful consideration. Furthermore, the observed constraint dependence of active depletion forces [58] and active pressure [62] underscores the need to explicitly incorporate this effect into theoretical models. Therefore, it is of great importance to investigate constraint dependence-induced corrections to the relationship between depletionlike forces and AP distributions, thereby generalizing the existing theoretical framework.

In this paper, we employ computational simulations to study the relationship between the effective force experienced by a passive particle constrained adjacent to the system boundary and the surrounding AP density distribution, under varying constraint strengths. We find that the previously established formula, which neglects the constraint factor [72], does not accurately capture the quantitative correlation between the effective force on passive objects subjected to weak constraints and the AP density distribution. We introduce different parameters to account for the constraint dependence of the microscopic AP distribution, successfully linking the distribution to the effective force on passive particles. This modified relation is supported by the consistency between theoretical predictions and simulation results across a broader parameter space.

## II. METHOD

### A. Simulation details

We consider a two-dimensional (2D) active bath consisting of small APs with diameter  $\sigma_s$  and a large passive probe with diameter of  $\sigma_l = 7.5\sigma_s$ , as the case of the previous experimental setup [72]. The schematic of the simulation system is shown in Fig. 1(a), where the APs, with a packing fraction of  $\rho = 0.3$ , are confined within a circular boundary of diameter  $50\sigma_s$ . To describe the pairwise interactions between particles separated by a distance  $r$ , we employ the repulsive Weeks Chandler-Andersen (WCA) potential [73], expressed as

$$U_{\text{WCA}}(r) = 4\epsilon \left[ \left( \frac{\sigma}{r} \right)^{24} - \left( \frac{\sigma}{r} \right)^{12} + \frac{1}{4} \right] \Theta(2^{1/12}\sigma - r), \quad (1)$$

where  $\epsilon$  is the interaction strength, set equal to the thermal energy  $k_B T$ , and  $\sigma$  denotes the length scale of the potential. The Heaviside step function  $\Theta(\cdot)$  ensures that the potential is activated only when the particles are within a certain distance. We take  $\sigma_{ss} = 2^{-1/12}\sigma_s$  and  $\sigma_{ls} = 2^{-13/12}(\sigma_l + \sigma_s)$  to calculate the potential between two small APs and between an AP and the large probe. The interaction between the APs and the circular confinement is modeled using  $\sigma_{sc} = 2^{-13/12}\sigma_s$ , while the probe-confinement interaction is described using  $\sigma_{lc} = 2^{-13/12}\sigma_l$ .

We model the translational and rotational motion of the APs using the underdamped Langevin equation,

$$m\dot{\mathbf{v}} = -\gamma_s \mathbf{v} + \mathbf{F}_d + \mathbf{F}_r + \boldsymbol{\eta}, \quad (2)$$

$$I\dot{\boldsymbol{\omega}} = -\gamma_r \boldsymbol{\omega} + \boldsymbol{\xi}, \quad (3)$$

where  $m$  is the particle mass,  $\gamma_s$  is the translational friction coefficient,  $\mathbf{F}_d$  and  $\mathbf{F}_r$  are the self-propulsion and steric repulsive forces,  $I$  is the moment of inertia, and  $\gamma_r = \sigma_s^2 \gamma_s / 3$  is the rotational friction coefficient. The stochastic terms  $\boldsymbol{\eta}$  and  $\boldsymbol{\xi}$  are Gaussian-distributed forces and torques, each with a mean of zero, and are correlated as  $\langle \eta_i(t) \eta_j(t') \rangle = 2k_B T \gamma_s \delta_{ij} \delta(t - t')$  and  $\langle \xi_i(t) \xi_j(t') \rangle = 2k_B T \gamma_r \delta_{ij} \delta(t - t')$ . The passive probe follows the same equation [Eq. (2)], except with  $\mathbf{F}_d = 0$ . In addition to its interactions with the APs, the probe is constrained by an external harmonic potential,  $U(\mathbf{r}_p) = \frac{1}{2}k(\mathbf{r}_p - \mathbf{r}_0)^2$ , where  $\mathbf{r}_0$  is the trap center, as shown in Fig. 1(b).

The time step for the numerical integration of the equations of motion is  $\Delta t = 10^{-3} \times \sigma_s \sqrt{m/\epsilon}$ . Throughout the paper, each data point in the figures corresponds to the results from eight independent trajectories, each consisting of  $3 \times 10^8$  steps, with a frame extracted every four steps for data analysis. All simulations are carried out in standard reduced units, where  $m$ ,  $\sigma_s/2$ , and  $\epsilon$  are taken as the units of mass, length, and energy, respectively.

### B. Theoretical framework for active effective force

The force exerted by the APs on the probe particle is calculated using the theoretical framework developed by Paul *et al.* [72], based on active stress [68–71]. In the absence of external constraints, the force along the  $x$  axis (due to symmetry) acting on the probe within a circular cavity is given by

$$F_x = C(r_b) k_B T_{\text{eff}}, \quad (4)$$

where the effective temperature  $k_B T_{\text{eff}}$  encodes the increased density fluctuations due to particle activity and is given by

$$k_B T_{\text{eff}} = k_B T \left[ 1 + \frac{v \tau_r \hat{v}}{2D_0} + \frac{D_0 \tau_r}{\xi^2} \frac{v}{\hat{v}} \left( \frac{\xi^2}{r_b^2} + \frac{\xi}{r_b} - 1 \right) \right]. \quad (5)$$

Here,  $D_0 = k_B T / \gamma_s$  is the translational diffusion constant and  $\tau_r = \gamma_r / k_B T$  is the rotational relaxation time.  $v$  is the self-propelled speed, while  $\hat{v}(\mathbf{r})$  is a spatially varying effective speed that considers the interactions with neighboring particles due to their excluded volume,  $\hat{v}(\mathbf{r}) = \hat{v}[\rho(\mathbf{r})]$ . The decay length  $\xi$  can be obtained by fitting the density profiles. Further details of the measurements for  $\hat{v}(\mathbf{r})$  and  $\xi$  are provided in the Supplemental Material [74].

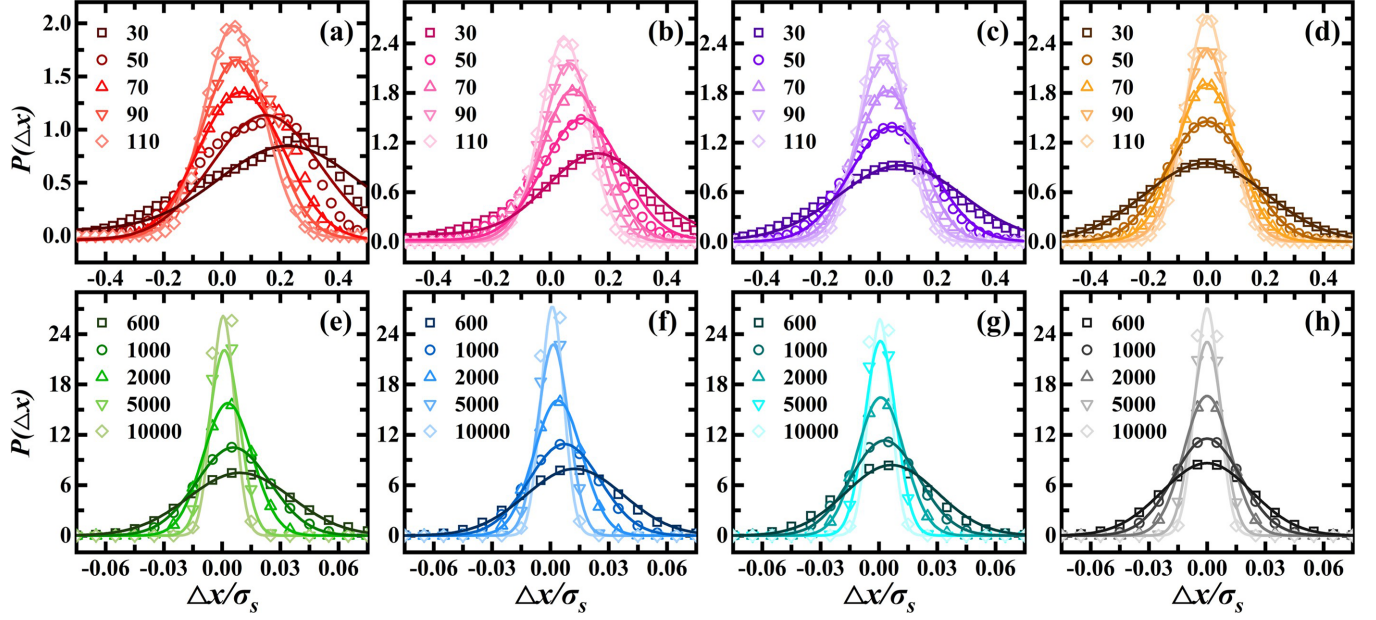


FIG. 2. Distribution  $P(\Delta x)$  for various probe-wall distances: (a), (e)  $d/\sigma_s = 1.25$ , (b), (f) 1.45, (c), (g) 2.45, and (d), (h) 4.25. Solid lines represent Gaussian fits to the data. Color depth indicates different constraint strengths applied to the probe, quantified by the harmonic spring coefficient  $k$ .

Additionally, the  $C(r_b)$  in Eq. (4) solely depends on the density of APs outside the probe, expressed as

$$C(r_b) = \int_0^{2\pi} d\varphi r_b \cos \varphi \rho(r_b, \varphi), \quad (6)$$

where  $r_b$  is the circular radius and  $\varphi$  is the angle used in the integration contour, as illustrated in Fig. 1(b). In this study, we set  $r_b = 0.5\sigma_l + 0.85\sigma_s$ , ensuring that  $r_b$  is large enough to completely enclose the probe, yet small enough to avoid the confinement, which is demonstrated by Paul *et al.* [72] that the integral  $C(r_b)$  remains largely unchanged over a range of  $r_b$  values.

### III. RESULTS AND DISCUSSION

#### A. The constraint dependence of probe and the surrounding AP distributions

We first reproduce and extend the simulations of Paul *et al.* [72], systematically varying the constraint strength applied to the passive probe. This approach enables us to reveal how both the probe's positional distribution and the surrounding AP density evolve under different constraint conditions—a key discrepancy not addressed in the previous study [72]. As shown in Figs. 2(a)–2(c), when the probe is weakly constrained, its position distribution markedly deviates from a Gaussian form. Conversely, Figs. 2(e)–2(g) show that for sufficiently strong constraints, the position distribution—or the small position fluctuations—can be well fitted by a Gaussian. This behavior directly results from the finite persistence length of the APs. When the dynamics of the passive tracer are easily perturbed, unbalanced collisions with APs lead to large positional fluctuations. However, under strong constraints, the passive tracer's motion is less affected by the APs and its behavior in the active bath becomes analogous to that

of a Brownian particle in a thermal bath at low temperatures. This is consistent with previous studies of probe energies in an active bath [59,60], where it was shown that under weak constraints, the probe's kinetic energy ( $mv_x^2/2$ ) and potential energy ( $k\Delta x^2/2$ ) significantly deviate from the equipartition theorem prediction ( $k_B T/2$ ). As the spring constant  $k$  increases, the energy distribution approaches the equilibrium value expected in a thermal bath.

Figures 2(d) and 2(h) show the scenario where the probe is distant from the boundary, resulting in relatively balanced collisions with the surrounding APs. Here, the position distribution remains nearly symmetric around the trap center. In contrast, when the probe is closer to the boundary, particularly under weaker constraint [Figs. 2(a)–2(c)], the peak of the position distribution shifts significantly to the right, indicating a larger gap between the probe and the boundary. This shift suggests that the constraint strength on the probe may affect not only its position distribution, but also the surrounding AP distribution.

The AP density distribution  $\rho(r_b, \varphi)$ , normalized by the global density  $\rho_0$ , is measured at a distance  $r_b$  from the probe [see Fig. 1(b)], as a function of the angle  $\varphi$  (Fig. 3). For any probe-wall distance in Figs. 3(a)–3(d), the AP density near  $\varphi = 0$  (where the probe is closest to the boundary) decreases significantly as the constraint strength weakens (i.e., as  $k$  decreases). This behavior arises from the persistence of motion in the APs, which become more easily trapped in the narrow gap between the passive tracer and the boundary. Under weak constraints, APs pass through the gap more freely. However, under stronger constraints, the passive tracer's displacement within the orientational diffusion time of the APs is insufficient, leading to significant accumulation of APs in the concave region. This behavior mirrors the previously studied dependence of the active depletion force on constraint strength [58].



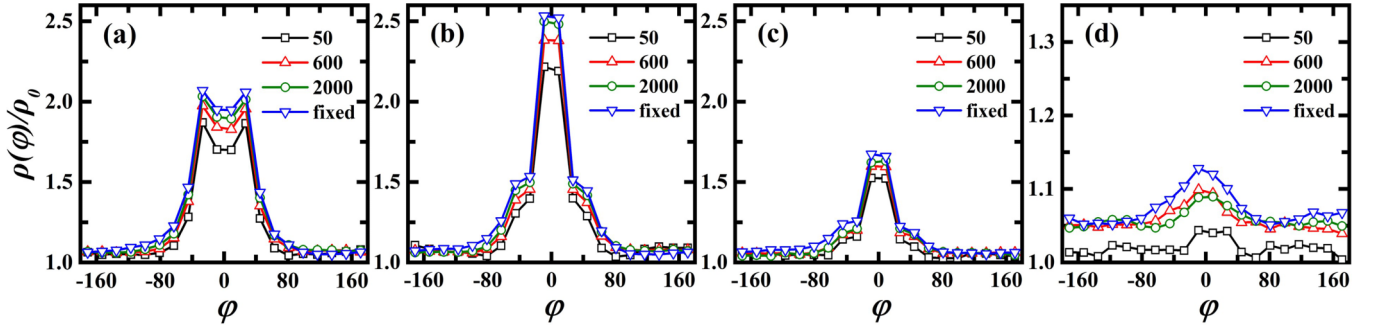


FIG. 3. Measured AP density distributions  $\rho(r_b, \varphi)$ , normalized by the mean number density  $\rho_0$ , with colors indicating different constraint strengths applied to the probe. (a)–(d) correspond to various probe-wall distances:  $d/\sigma_s = 1.25, 1.45, 2.45$  and  $4.25$ , respectively.

Additionally, in Fig. 3(a), where the probe is close to the boundary, the double-peaked structure of the curves indicates significant accumulation of APs within the gap between the probe and the wall. As the probe-wall distance increases [Figs. 3(b)–3(d)], the peak value of  $\rho(r_b, \varphi)$  decreases, as a dynamic bridge of multiple AP layers between the probe and the wall cannot be maintained in dilute suspensions [51]. For large probe-wall distances and weak constraints on the probe, such as the black line in Fig. 3(d), the sufficient displacement within the orientational diffusion time of the swimmers prevents APs from accumulating, resulting in a more uniform distribution of APs. In summary, the microscopic distribution of APs is highly sensitive to the constraint strength applied to the probe, affecting the integral  $C(r_b)$  in Eq. (4). Consequently, as the constraint strength changes, the relationship between  $F_x$  (which relates to the probe deviations shown in Fig. 2) and  $C(r_b)$  (which is associated with the AP density distribution in Fig. 3) may not always maintain quantitative consistency.

### B. The relationship between the effective force and the constraint-dependent AP distribution

As illustrated in Fig. 4(a), we measure the effective force  $F_x$  on the probe as a function of normalized distance  $d/\sigma_s$  under various constraint strengths  $k$ . In general, both simulation results (solid symbols) and theoretical predictions from Eq. (4) (open symbols) exhibit a nonmonotonic, oscillatory decay, consistent with prior experimental and theoretical studies [51,53,54,58,72,75]. Notably, for larger values of  $k$ , the simulation results and theoretical predictions align very well. However, for smaller values of  $k$ , a substantial discrepancy emerges between the simulated and predicted  $F_x$ . In Fig. 4(c), we highlight the differences in the peak values of  $F_x$  from Fig. 4(a) for various  $k$ . When the probe is subjected to a strong constraint or is fixed (indicated by dashed lines), the theoretical and simulated values of  $F_x$  quantitatively agree with each other. As the constraint strength  $k$  decreases, however, the discrepancy becomes more pronounced, reaching a more than threefold difference. This suggests that the prediction of the effective force on the probe via the AP distribution from Eq. (4) is more accurate at higher constraint strengths.

According to the above findings, the good agreement between the theory and the experiment by Paul *et al.* [72] means that the probe is subjected to a significant constraint, which

mainly arises from the following three aspects. First, the optical trap imposes a harmonic potential that restricts its motion. Second, the probe, with a size of  $15\ \mu\text{m}$ —significantly larger than the surrounding APs ( $2\ \mu\text{m}$ )—experiences strong hydrodynamic friction from the surrounding fluid. Third, the four supporting legs of the probe further contribute additional friction with the substrate. Collectively, these effects—optical trapping, fluid-induced friction, and substrate

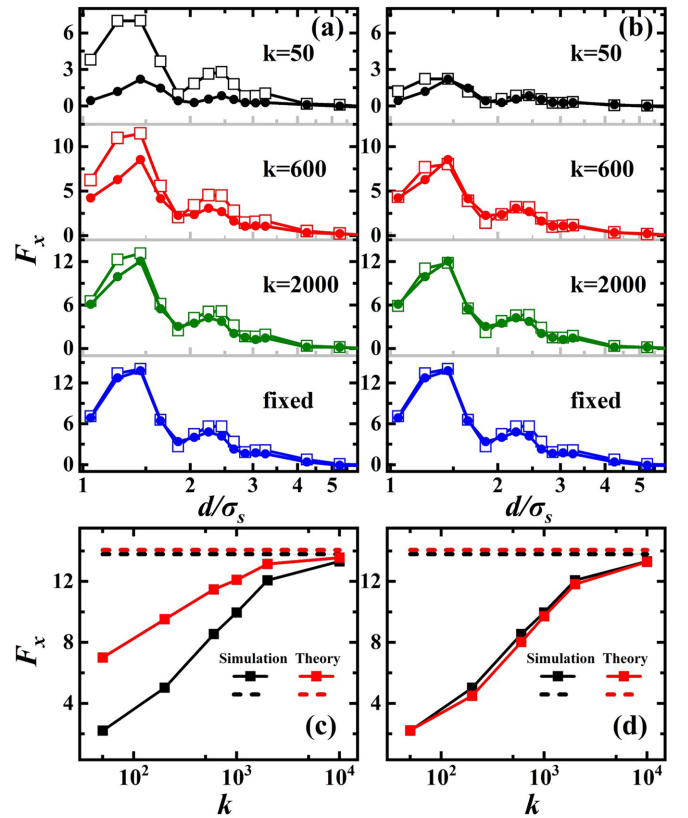


FIG. 4. (a) Comparison of  $F_x$  as a function of normalized distance  $d/\sigma_s$  under various constraint strengths  $k$ , between simulation results (solid symbols) and the prediction from Eq. (4) (open symbols). (b) Comparison of  $F_x$  between simulation results (solid symbols) and the generalized prediction based on Eq. (8) (open symbols). (c), (d) The comparison of the peak values of  $F_x$  from (a) and (b), respectively. The dashed lines in (c) and (d) represent the case of fixed passive probe, i.e., when  $k \rightarrow \infty$ .

friction—severely restrict the probe’s mobility. Moreover, achieving weak optical constraints in experiments remains challenging, as collisions with APs may displace the probe beyond the optical trap’s measurement range, thereby hindering accurate force quantification.

Building upon Eq. (4) from Paul *et al.* [72], we seek to integrate the constraint factor into the relationship between the effective force on the probe and the surrounding AP distribution. In our previous study [62], the average pressure exerted by a single AP on the probe under various constraint strengths was predicted as

$$P_s = C_1 \frac{\mathbf{F}_d}{\pi \sigma_l} \left\{ 1 + \frac{\gamma_s}{k\tau_r} [e^{-k\tau_r/(\gamma_l + \gamma_s)} - 1] \right\}, \quad (7)$$

which captures the average effect of AP collisions with the probe over the characteristic time  $\tau_r$ . The fitting parameter  $C_1$  arises from the assumption of central collisions between a single AP and the probe. We now apply this modified pressure term from Eq. (7) to correct the effective force on the passive probe described by Eq. (4),

$$F_x = \beta C(r_b) k_B T_{\text{eff}}, \quad (8)$$

where

$$\beta = 1 + \frac{C_1 \gamma_s}{C_2 k \tau_r} [e^{-C_2 k \tau_r / (\gamma_l + \gamma_s)} - 1]. \quad (9)$$

Here, two fitting parameters are introduced:  $C_1 = 1.85$ , which corrects for deviations due to the central collision assumption [as in Eq. (7)], and  $C_2 = 0.0085$ , which adjusts for the influence of the probe’s constraint strength on the accumulation of surrounding APs. Notably, both parameters are independent of any constraints—whether the external constraint imposed on the probe, represented by  $k$ , or the environmental constraint from the thermal bath, reflected by the probe’s translational friction coefficient  $\gamma_l$ . In the limiting cases where  $k \rightarrow \infty$  or  $\gamma_l \rightarrow \infty$ , the probe effectively becomes immobilized due to either an external trapping force or hydrodynamic resistance, leading to  $\beta = 1$  and the reduction of Eq. (8) to Eq. (4). In the opposite limit  $k \rightarrow 0$ , the effective force substantially decreases, consistent with the reduced AP accumulation and weaker repulsion. These physically meaningful limits support the validity of our proposed correction. Importantly, the parameters  $C_1$  and  $C_2$  are independent of constraint strength  $k$  or  $\gamma_l$  once other parameters of the system are given (with  $F_d$ ,  $\tau_r$ , and  $\rho$  specified). Therefore, the fitting can be consistently performed across all the simulations presented in Fig. 4. Determining  $C_1$  and  $C_2$  from first principles would require knowledge of the temporal and spatial distribution of the surrounding APs under varying constraints, which cannot be analytically derived due to the inherently nonequilibrium and many-body nature of these complex active systems. Figure 4(b) compares the simulation results (solid symbols) with the predictions from Eq. (8) (open symbols), while Fig. 4(d) shows the comparison of the peak values of  $F_x$  from Fig. 4(b) for various  $k$ . The results are in excellent agreement, demonstrating that the effective force on the probe is more robustly linked to the surrounding AP density distribution, as corrected by the constraint factor  $\beta$ . For comparison, simulation results obtained using the conventional 12-6 WCA potential are provided in the Supplemental Material [74].

By exploring a broader parameter space, we further elucidate the relationship between the effective force  $F_x$  and constraint-dependent AP distribution  $\beta C(r_b)$ . The persistence length of the APs is tuned by adjusting both the driving force  $\mathbf{F}_d$  and the rotational relaxation time  $\tau_r = \gamma_r / k_B T$  (while keeping  $k_B T = \epsilon$  constant), both of which contribute to an increase in the persistence length. Previous studies have demonstrated that while the persistence length depends similarly on  $\mathbf{F}_d$  and  $\tau_r$ , their effects on key transport properties, such as the effective diffusion coefficient of a single AP [76] or the active depletion force between two probes [58], are not quantitatively equivalent. In this work, the comparison of  $F_x$  between simulation results (solid symbols) and predictions from Eq. (8) (open symbols) under varying  $\mathbf{F}_d$  is shown in Figs. 5(a1)–5(a4), and, similarly, comparisons under different rotational relaxation times  $\tau_r$  are displayed in Figs. 5(b1)–5(b4). Across all cases, these comparisons exhibit excellent agreement, reinforcing the robustness of the proposed model. This consistency also holds under different AP packing fractions  $\rho$ , shown in Figs. 5(c1)–5(c4), despite notable differences in the microscopic AP distributions, including clustering and dynamic crystalline bridge formation between passive objects at varying  $\rho$  [51,57]. The corresponding values of  $C_1$  and  $C_2$  for different  $F_d$ ,  $\tau_r$ , and  $\rho$  are provided in the Supplemental Material [74]. Thus, Fig. 5 demonstrates that by incorporating the constraint factor  $\beta$ , the relationship between the effective force  $F_x$  and constraint-dependent AP distribution  $\beta C(r_b)$  can be generalized across a broader physical parameter space.

Finally, we emphasize that the parameters  $C_1$  and  $C_2$  are uniquely determined for a given system, allowing for explicit calculation of the constraint factor  $\beta$  in limiting cases. Taking Fig. 5(a4) as an example, we find  $\beta = 1$  for  $k \rightarrow \infty$ , corresponding to a fixed probe, while for  $k \rightarrow 0$ , we obtain  $\beta = 0.09$ . This approximately 10-fold variation in the correction factor  $\beta$  between the strongest and weakest constraint limits can be interpreted as follows. Under strong constraints, the passive probe exhibits minimal displacement within the orientational diffusion time of the APs, leading to pronounced accumulation of APs in the concave region between the probe and the nearby boundary. This localized AP accumulation enhances persistent AP-probe collisions, resulting in stronger repulsive forces. Such behavior is analogous to the formation of dense microstructures observed between two plates in an active bath by Ni *et al.* [51]. Conversely, in the weak constraint limit, the probe undergoes large fluctuations in response to AP collisions. This increased mobility allows APs to easily pass through the concave gap region, substantially reducing local AP accumulation and weakening the persistence of AP-probe interactions. As a result, the variation in the correction factor  $\beta$  reflects a substantial and meaningful effect, underscoring the critical importance of incorporating the constraint factor  $\beta$  to generalize the relationship between  $F_x$  and  $C(r_b)$ .

#### IV. CONCLUSIONS

By introducing a constraint-dependent correction factor into the existing theory, we establish a more precise relationship between AP density distributions and the effective force on a probe under varying external constraints. Our

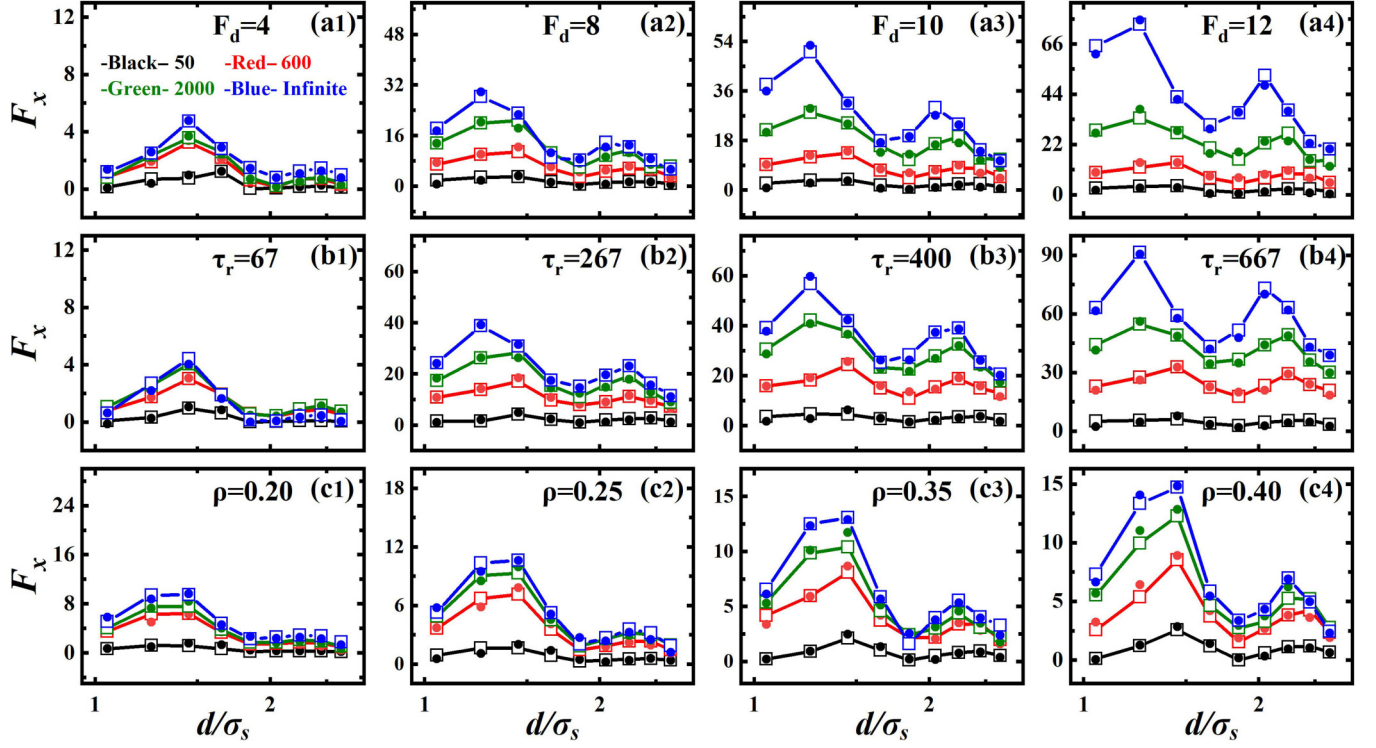


FIG. 5. Comparison of the effective force  $F_x$  as a function of normalized distance  $d/\sigma_s$  under various constraint strengths  $k$ , between simulation results (solid symbols) and the predictions from Eq. (8) (open symbols) with consistent fitting parameters. (a1)–(a4) Variations in the self-propelled force of the APs,  $F_d = 4, 8, 10$ , and  $12$ ; (b1)–(b4) different rotational relaxation times of the APs,  $\tau_r = 67, 267, 400$ , and  $667$ ; (c1)–(c4) the effects of varying AP packing fractions,  $\rho = 0.20, 0.25, 0.35$ , and  $0.40$ . The benchmark parameters are fixed at  $F_d = 6$ ,  $\tau_r = 133$ , and  $\rho = 0.30$ , unless otherwise specified.

framework attains excellent agreement between theoretical predictions and simulations across a broad parameter space. These findings yield a generalized understanding of constraint-dependent forces in active matter, offering vital insights for experiments where intrinsic constraints, such as optical tweezer confinement, may influence measurements. This work enhances the theoretical foundation of active matter interactions, paving the way for experimental validation and the controlled manipulation of nonequilibrium forces.

#### ACKNOWLEDGMENTS

We acknowledge the support of the National Natural Science Foundation of China (Grants No. 12374205, No. 12304245, No. T2325027, No. 12274448, and No.

12475031), the Natural Science Foundation of Shandong Province (Grant No. ZR2024YQ017), the Science Foundation of China University of Petroleum, Beijing (Grants No. 2462023YJRC031 and No. 2462024BJRC010), the National Key Laboratory of Petroleum Resources and Engineering (Grant No. PRE/DX-2407), the Young Elite Scientist Sponsorship Program by BAST (Grant No. BYESS2023300), and the Beijing Institute of Technology Research Fund Program for Young Scholars. This work was also supported by Beijing National Laboratory for Condensed Matter Physics (Grants No. 2023BNLCMPKF014 and No. 2024BNLCMPKF009).

#### DATA AVAILABILITY

The data that support the findings of this article are available upon request.

- 
- [1] M. C. Marchetti, J. F. Joanny, S. Ramaswamy, T. B. Liverpool, J. Prost, M. Rao, and R. A. Simha, *Rev. Mod. Phys.* **85**, 1143 (2013).
  - [2] A. Rigato, A. Miyagi, S. Scheuring, and F. Rico, *Nat. Phys.* **13**, 771 (2017).
  - [3] J. Toner and Y. Tu, *Phys. Rev. Lett.* **75**, 4326 (1995).
  - [4] R. D. Vale, *Cell* **112**, 467 (2003).
  - [5] M. Schliwa and G. Woehlke, *Nature (London)* **422**, 759 (2003).
  - [6] A. J. W. Ward, D. J. T. Sumpter, I. D. Couzin, P. J. B. Hart, and J. Krause, *Proc. Natl. Acad. Sci. USA* **105**, 6948 (2008).
  - [7] M. Ballerini, N. Cabibbo, R. Candelier, A. Cavagna, E. Cisbani, I. Giardina, V. Lecomte, A. Orlandi, G. Parisi, A. Procaccini *et al.*, *Proc. Natl. Acad. Sci. USA* **105**, 1232 (2008).
  - [8] H. P. Zhang, A. Be'er, E.-L. Florin, and H. L. Swinney, *Proc. Natl. Acad. Sci. USA* **107**, 13626 (2010).



- [9] H. Wioland, F. G. Woodhouse, J. Dunkel, J. O. Kessler, and R. E. Goldstein, *Phys. Rev. Lett.* **110**, 268102 (2013).
- [10] E. Lushi, H. Wioland, and R. E. Goldstein, *Proc. Natl. Acad. Sci. USA* **111**, 9733 (2014).
- [11] X. Chen, X. Yang, M. Yang, and H. P. Zhang, *Europhys. Lett.* **111**, 54002 (2015).
- [12] A. Cavagna, D. Conti, C. Creato, L. Del Castello, I. Giardina, T. S. Grigera, S. Melillo, L. Parisi, and M. Viale, *Nat. Phys.* **13**, 914 (2017).
- [13] R. Alert and X. Trepát, *Annu. Rev. Condens. Matter Phys.* **11**, 77 (2020).
- [14] A. Be'er, B. Ilkanaiv, R. Gross, D. B. Kearns, S. Heidenreich, M. Bär, and G. Ariel, *Commun. Phys.* **3**, 66 (2020).
- [15] W. F. Paxton, K. C. Kistler, C. C. Olmeda, A. Sen, S. K. St. Angelo, Y. Cao, T. E. Mallouk, P. E. Lammert, and V. H. Crespi, *J. Am. Chem. Soc.* **126**, 13424 (2004).
- [16] J. R. Howse, R. A. L. Jones, A. J. Ryan, T. Gough, R. Vafabakhsh, and R. Golestanian, *Phys. Rev. Lett.* **99**, 048102 (2007).
- [17] H.-R. Jiang, N. Yoshinaga, and M. Sano, *Phys. Rev. Lett.* **105**, 268302 (2010).
- [18] I. Theurkauff, C. Cottin-Bizonne, J. Palacci, C. Ybert, and L. Bocquet, *Phys. Rev. Lett.* **108**, 268303 (2012).
- [19] J. Palacci, S. Sacanna, A. P. Steinberg, D. J. Pine, and P. M. Chaikin, *Science* **339**, 936 (2013).
- [20] C. Lozano, B. Ten Hagen, H. Löwen, and C. Bechinger, *Nat. Commun.* **7**, 12828 (2016).
- [21] V. Narayan, S. Ramaswamy, and N. Menon, *Science* **317**, 105 (2007).
- [22] S. Ramaswamy, *Annu. Rev. Condens. Matter Phys.* **1**, 323 (2010).
- [23] C. A. Weber, T. Hanke, J. Deseigne, S. Léonard, O. Dauchot, E. Frey, and H. Chaté, *Phys. Rev. Lett.* **110**, 208001 (2013).
- [24] O. Dauchot and V. Démery, *Phys. Rev. Lett.* **122**, 068002 (2019).
- [25] T. Vicsek and A. Zafeiris, *Phys. Rep.* **517**, 71 (2012).
- [26] H. H. Wensink, J. Dunkel, S. Heidenreich, K. Drescher, R. E. Goldstein, H. Löwen, and J. M. Yeomans, *Proc. Natl. Acad. Sci. USA* **109**, 14308 (2012).
- [27] A. Bricard, J.-B. Caussin, N. Desreumaux, O. Dauchot, and D. Bartolo, *Nature (London)* **503**, 95 (2013).
- [28] J. Elgeti, R. G. Winkler, and G. Gompper, *Rep. Prog. Phys.* **78**, 056601 (2015).
- [29] J. Yan, M. Han, J. Zhang, C. Xu, E. Luijten, and S. Granick, *Nat. Mater.* **15**, 1095 (2016).
- [30] G. Kokot, S. Das, R. G. Winkler, G. Gompper, I. S. Aranson, and A. Snezhko, *Proc. Natl. Acad. Sci. USA* **114**, 12870 (2017).
- [31] A. Deblais, T. Barois, T. Guérin, P. H. Delville, R. Vaudaine, J. S. Lintuvuori, J. F. Boudet, J. C. Baret, and H. Kellay, *Phys. Rev. Lett.* **120**, 188002 (2018).
- [32] H. Massana-Cid, F. Meng, D. Matsunaga, R. Golestanian, and P. Tierno, *Nat. Commun.* **10**, 2444 (2019).
- [33] I. Buttinoni, J. Bialké, F. Kümmel, H. Löwen, C. Bechinger, and T. Speck, *Phys. Rev. Lett.* **110**, 238301 (2013).
- [34] M. E. Cates and J. Tailleur, *Annu. Rev. Condens. Matter Phys.* **6**, 219 (2015).
- [35] E. Sesé-Sansa, I. Pagonabarraga, and D. Levis, *Europhys. Lett.* **124**, 30004 (2018).
- [36] A. P. Solon, Y. Fily, A. Baskaran, M. E. Cates, Y. Kafri, M. Kardar, and J. Tailleur, *Nat. Phys.* **11**, 673 (2015).
- [37] F. Smallenburg and H. Löwen, *Phys. Rev. E* **92**, 032304 (2015).
- [38] D. Loi, S. Mossa, and L. F. Cugliandolo, *Phys. Rev. E* **77**, 051111 (2008).
- [39] J. Palacci, C. Cottin-Bizonne, C. Ybert, and L. Bocquet, *Phys. Rev. Lett.* **105**, 088304 (2010).
- [40] D. Loi, S. Mossa, and L. F. Cugliandolo, *Soft Matter* **7**, 3726 (2011).
- [41] G. Szamel, *Phys. Rev. E* **90**, 012111 (2014).
- [42] S. C. Takatori, W. Yan, and J. F. Brady, *Phys. Rev. Lett.* **113**, 028103 (2014).
- [43] F. Ginot, I. Theurkauff, D. Levis, C. Ybert, L. Bocquet, L. Berthier, and C. Cottin-Bizonne, *Phys. Rev. X* **5**, 011004 (2015).
- [44] T. Speck, *Europhys. Lett.* **114**, 30006 (2016).
- [45] É. Fodor, C. Nardini, M. E. Cates, J. Tailleur, P. Visco, and F. van Wijland, *Phys. Rev. Lett.* **117**, 038103 (2016).
- [46] D. Mandal, K. Klymko, and M. R. DeWeese, *Phys. Rev. Lett.* **119**, 258001 (2017).
- [47] S. Asakura and F. Oosawa, *J. Polym. Sci.* **33**, 183 (1958).
- [48] A. Vrij, *Pure Appl. Chem.* **48**, 471 (1976).
- [49] J. Harder, S. A. Mallory, C. Tung, C. Valeriani, and A. Cacciuto, *J. Chem. Phys.* **141**, 194901 (2014).
- [50] D. Ray, C. Reichhardt, and C. J. Olson Reichhardt, *Phys. Rev. E* **90**, 013019 (2014).
- [51] R. Ni, M. A. Cohen Stuart, and P. G. Bolhuis, *Phys. Rev. Lett.* **114**, 018302 (2015).
- [52] L. R. Leite, D. Lucena, F. Q. Potiguar, and W. P. Ferreira, *Phys. Rev. E* **94**, 062602 (2016).
- [53] M. Z. Yamchi and A. Naji, *J. Chem. Phys.* **147**, 194901 (2017).
- [54] A. Duzgun and J. V. Selinger, *Phys. Rev. E* **97**, 032606 (2018).
- [55] Y. Hua, K. Li, X. Zhou, L. He, and L. Zhang, *Soft Matter* **14**, 5205 (2018).
- [56] Y. Baek, A. P. Solon, X. Xu, N. Nikola, and Y. Kafri, *Phys. Rev. Lett.* **120**, 058002 (2018).
- [57] L. Ning, X. Lou, Q. Ma, Y. Yang, N. Luo, K. Chen, F. Meng, X. Zhou, M. Yang, and Y. Peng, *Phys. Rev. Lett.* **131**, 158301 (2023).
- [58] P. Liu, S. Ye, F. Ye, K. Chen, and M. Yang, *Phys. Rev. Lett.* **124**, 158001 (2020).
- [59] S. Ye, P. Liu, Z. Wei, F. Ye, M. Yang, and K. Chen, *Chin. Phys. B* **29**, 058201 (2020).
- [60] S. Ye, P. Liu, F. Ye, K. Chen, and M. Yang, *Soft Matter* **16**, 4655 (2020).
- [61] L. Li, P. Liu, K. Chen, N. Zheng, and M. Yang, *Soft Matter* **18**, 4265 (2022).
- [62] P. Liu, L. Li, L. Ning, N. Zheng, and M. Yang, *J. Phys.: Condens. Matter* **35**, 445102 (2023).
- [63] S. Asakura and F. Oosawa, *J. Chem. Phys.* **22**, 1255 (1954).
- [64] Y. Mao, M. E. Cates, and H. N. W. Lekkerkerker, *Physica A* **222**, 10 (1995).
- [65] B. Götzmann, R. Evans, and S. Dietrich, *Phys. Rev. E* **57**, 6785 (1998).
- [66] C. P. Royall, D. G. A. L. Aarts, and H. Tanaka, *J. Phys.: Condens. Matter* **17**, S3401 (2005).
- [67] D. Kleshchanok, R. Tuinier, and P. R. Lang, *J. Phys.: Condens. Matter* **20**, 073101 (2008).
- [68] A. P. Solon, J. Stenhammar, R. Wittkowski, M. Kardar, Y. Kafri, M. E. Cates, and J. Tailleur, *Phys. Rev. Lett.* **114**, 198301 (2015).

- [69] T. Speck, *Soft Matter* **16**, 2652 (2020).
- [70] T. Speck and A. Jayaram, *Phys. Rev. Lett.* **126**, 138002 (2021).
- [71] T. Speck, *Phys. Rev. E* **103**, 012607 (2021).
- [72] S. Paul, A. Jayaram, N. Narinder, T. Speck, and C. Bechinger, *Phys. Rev. Lett.* **129**, 058001 (2022).
- [73] J. D. Weeks, D. Chandler, and H. C. Andersen, *J. Chem. Phys.* **54**, 5237 (1971).
- [74] See Supplemental Material at <http://link.aps.org/supplemental/10.1103/rlp5-wxpf> for additional simulation details, which includes Refs. [69,70,72].
- [75] L. Angelani, C. Maggi, M. L. Bernardini, A. Rizzo, and R. Di Leonardo, *Phys. Rev. Lett.* **107**, 138302 (2011).
- [76] C. Bechinger, R. Di Leonardo, H. Löwen, C. Reichhardt, G. Volpe, and G. Volpe, *Rev. Mod. Phys.* **88**, 045006 (2016).